Inferring the Sun's Far-Side Magnetic Flux for Operations Using Time-Distance Helioseismic Imaging

S.A. Hess Webber[1] ✉, J. Zhao[1], R. Chen[1], J. T. Hoeksema[1], Y. Liu[1], M. Bobra[1] and M. DeRosa[2]

[1]W. W. Hansen Experimental Physics Laboratory, Stanford University, Stanford, CA, USA;
[2]Lockheed Martin Solar and Astrophysics Laboratory, Palo Alto, CA, USA;
Correspondence to: *shessweb@stanford.edu*

Solar wind models are highly dependent on global magnetic fields at the solar surface as their inner boundary condition, and the lack of global field data is a significant problem plaguing solar wind modeling. Currently, only direct observations of the near-side magnetic field exist and far-side approximations are incapable of predicting growth of existing active regions or new magnetic flux emergence. To fill this data gap, we develop a method that calibrates far-side helioseismic images, which are calculated using near-side Doppler observations, to far-side magnetic flux maps. The calibration employs multiple machine-learning methods that use EUV 304 Å data as a bridge. These algorithms determine a relation 1) between the near-side AIA 304 Å data and HMI magnetic field data, and 2) between STEREO 304 Å data and far-side helioseismic images obtained from a newly developed time-distance helioseismic far-side imaging method. The resulting magnetic flux maps have been further calibrated using maps produced by a flux transport model. The various data products from this work – far-side acoustic maps, far-side STEREO EUV-derived magnetic flux maps, and near-real-time acoustically-driven far-side magnetic flux maps, along with maps of the associated uncertainties – are being made available to enable a synchronic global magnetic flux input into coronal and solar wind models.

Background & Motivation

Reliable, near-real-time solar far-side magnetic flux maps are important for improved modeling of the background solar wind and the solar wind structure.

The following figure shows two synchronic maps (top) of magnetic field, one from data assimilation using only a flux transport model (FTM) [6] and the other after manually incorporating a large AR on the modeled data at the location of new emergence. The synchronic maps are used to calculate maps of Squashing factor Q (Q-maps; middle) [7] at a distance of 2.5 R_{sun}, employing a potential field source surface (PFSS) model [*e.g.* 1; 3; 5]. Q-maps effectively show magnetic topology. Lanes between opposite-sign (blue and red) regions in the maps represent current sheets (helmet streamers). Those between same-sign (same color) regions represent coronal hole boundaries (pseudo-streamers). The new active region (AR) changes the coronal structure significantly: altering the shapes of the existing pseudo-streamers (B and C), and generating a new pseudo-streamer (D). The "existing" and new pseudo-streamer are compared side-by-side with SOHO/LASCO C2 observations (bottom).

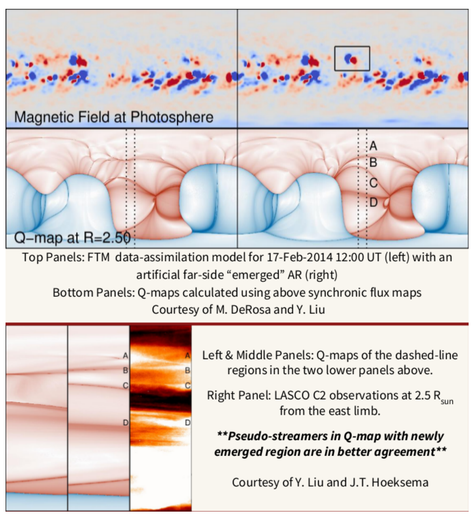

Top Panels: FTM data-assimilation model for 17-Feb-2014 12:00 UT (left) with an artificial far-side "emerged" AR (right)
Bottom Panels: Q-maps calculated using above synchronic flux maps
Courtesy of M. DeRosa and Y. Liu

Flux transport models. FTMs effectively progress observed near-side magnetic flux around to the solar far side. They provide reasonable approximations of the synchronic, full-sun signed flux based on assimilated magnetic data. Unfortunately, **FTMs are incapable of incorporating either the growth of existing ARs or the emergence of new magnetic flux.**

Far-side observations.
There is a quantitative relationship between 304 Å EUV emission and magnetic flux [8]. The STEREO/SECCHI EUVI instruments provide several years of far-side 304 Å observations (see example **below, bottom**). However, the STEREO spacecraft have already orbited back around to a separation angle $<90°$ with Earth. Furthermore, communications with STEREO B were permanently lost in Oct 2014, just before it passed behind the Sun. No current or planned missions have orbital positions conducive to consistent observations of the solar far side, either for magnetic fields or EUV proxies. **There is no guarantee of future observations.**

STEREO A & B spacecraft as of 2019-Sep-12 21:00 UT

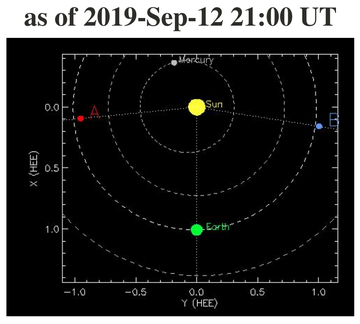

Credit: STEREO Science Center

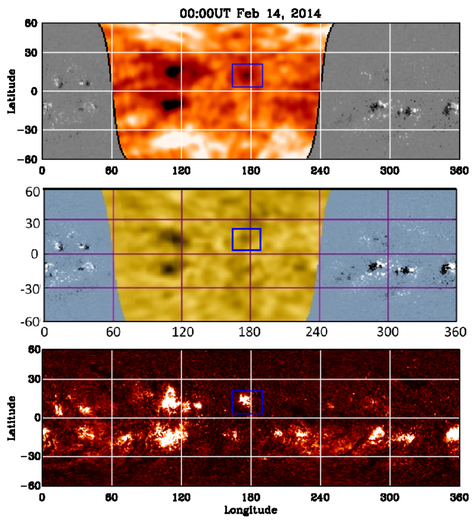

Helioseismic imaging.
Helioseismic techniques are also used to image the far side. These techniques include acoustic holography (middle) [2; 4] and time-distance methods [9]. These maps show the location and size of far-side ARs, but both methods often give spurious signals. We recently developed a new time-distance technique that increases the acoustic resolution of the far side maps (top) [10]. However, all acoustic maps are measures of wave travel-time perturbations. **None of these data are calibrated into magnetic flux.**

Data & Preparation

There are several overarching steps necessary to calibrate acoustic maps to far-side magnetic flux maps: (**bold teal** indicates available data product)

1. Generate **far-side acoustic travel-time maps** ✓✓
2. Use deep neural net to learn relationship between EUV and magnetic flux – using near-side images ✓✓
3. Apply learned EUV⇔magnetic-flux relationship to far-side EUV images to get **EUV-derived far-side magnetic flux proxy maps** ✓✓
4. Use deep neural net to learn relationship between far-side magnetic-flux proxy and far-side acoustic maps ✓
5. Apply learned far-side acoustic⇔magnetic-flux-proxy relationship to all acoustic maps to get **near-real-time acoustically-derived far-side magnetic flux maps** (current)
6. Use various data and model evaluation metrics to produce **associate uncertainty maps**

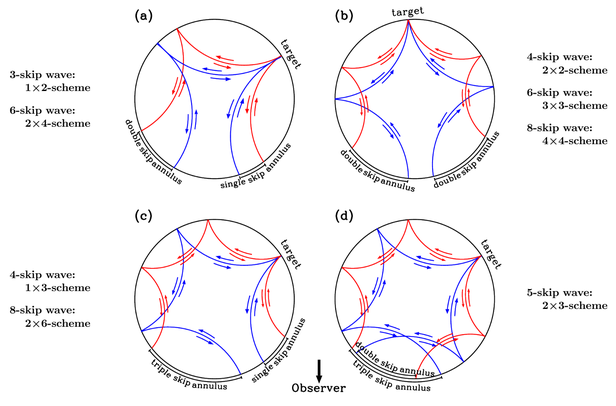

Producing far-side acoustic maps. Waves that get reflected within a far-side AR experience a reduction in their total travel times, which can be measured using near-side waves to show the location, size, and perhaps magnetic-field strength of the far-side AR. Our new far-side time-distance technique takes advantage of helioseismic geometry for different "skip" waves (number of surface reflections; *e.g.*, some 6- and 8-skip waves have the same far-side sensitivity geometry as 4-skip 2x2-scheme waves). We ultimately use 14 total sets of individual wave measurements to build up maps of acoustic wave travel-times across the far-side of the solar disk. The higher acoustic resolution requires less time-averaging for reliable signal-to-noise.

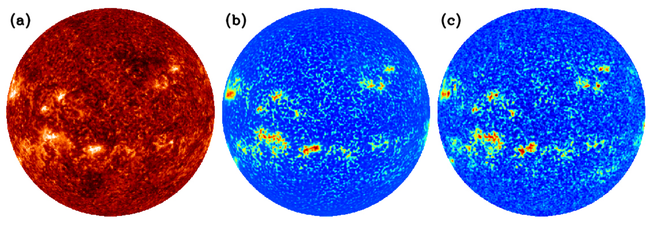

Machine learning between SDO/AIA and SDO/HMI. In order to convert *far-side* EUV 304 Å images to magnetic flux proxy data, we first train on corresponding *near-side* EUV 304 Å and magnetic flux images. We use a Unet deep learning architecture, trained on 4 image pairs of EUV and magnetic flux per day using 8 years of data from 2010-May 1 to 2018-Apr-30, a total of $\sim 11,000$ examples. Data are split into a training set, devel. set (4%), and test set (4%). 15 days are blocked before and after each devel./test set, to prevent the same ARs from appearing in both the training set, and development and test sets. **The trained deep neural network reproduces the magnetic flux in great detail from the EUV 304 Å flux, with a correlation of about 0.9.** The above example shows (a) an AIA 304 Å image (input), (b) the learned magnetic-flux proxy image (output), and (c) the actual HMI magnetic flux image (target).

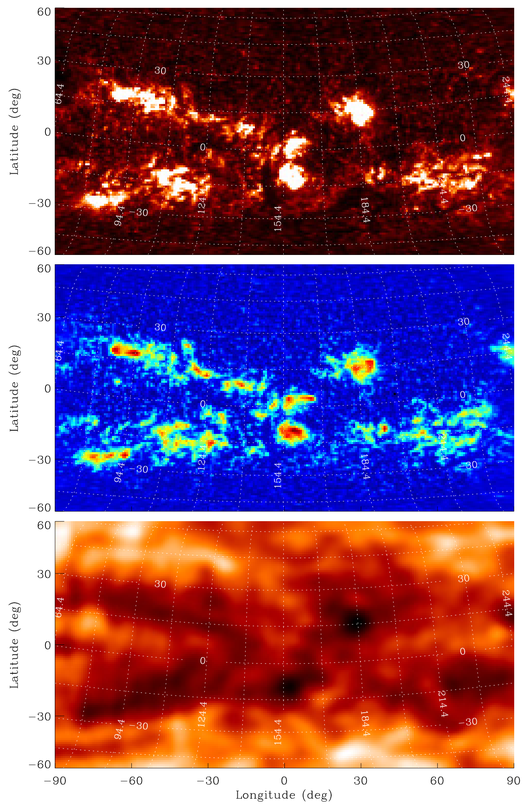

Prepped far-side data. Our far-side data sets are STEREO A & B EUVI 304 Å images (top), **derived STEREO A & B magnetic-flux proxy images (middle), and far-side acoustic images (bottom)**; this example is from 2014-May-13 00:00 UT. Both time-series range from 2010-May-13 00:00 UT–2014-Aug-18 12:00 UT (limited by availability of STEREO data). We include 2 observations per day (midnight & noon; UTC). After "bad" data are removed from the training set (partial images, flare occurrences, *etc.*), we ultimately train on a total of ~ 2500 pairs of images. Our maps have dimensions of 255✕121 (limited by the spatial resolution of acoustic maps). All images are in the form of far-side Carrington maps, using Carrington longitude (central meridian fixed at $0°$; between $\pm 90°$) and $\sin(\text{latitude})$ between $\pm 60°$.

Machine Learning Frameworks

Near-side EUV⇔Mag-Flux

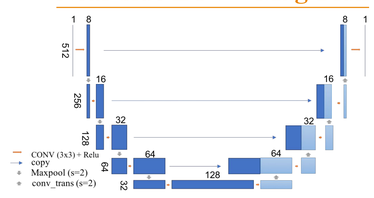

Far-side Mag Proxy⇔Acoustic

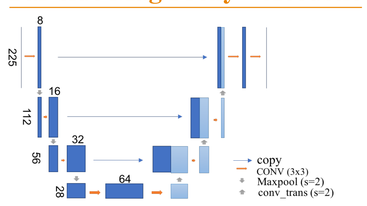

Unet deep neural network architecture. We use two Unet neural network models as training algorithms. **Unet combines local and global spatial information effectively.** Because of the relatively small training set for the STEREO images and the lower dimensionality of the acoustic images, we must use fewer convolutional layers in this framework than are used for the near-side architecture. In both architectures, a rectified linear unit (ReLU) non-linear mapping is applied after each 3×3 convolution, followed by a 2×2 maxpool downsampling. Through each downsampling step, feature channels are doubled. After the lowest convolutional layer, 2×2 convolutional upsampling is applied. Between each upsampling step, we concatenate the upsampled and downsampled channels of that convolutional layer, and perform a 3×3 convolution followed by a ReLU. Through each upsampling step, feature channels are halved. The final output map has the same dimensions as the original input map.

Results

Note, these acoustically-derived far-side magnetic flux maps results are preliminary. We have not yet compared between the output predictions and target images, or tweaked our initial Unet framework to improve performance. However, the results are promising!

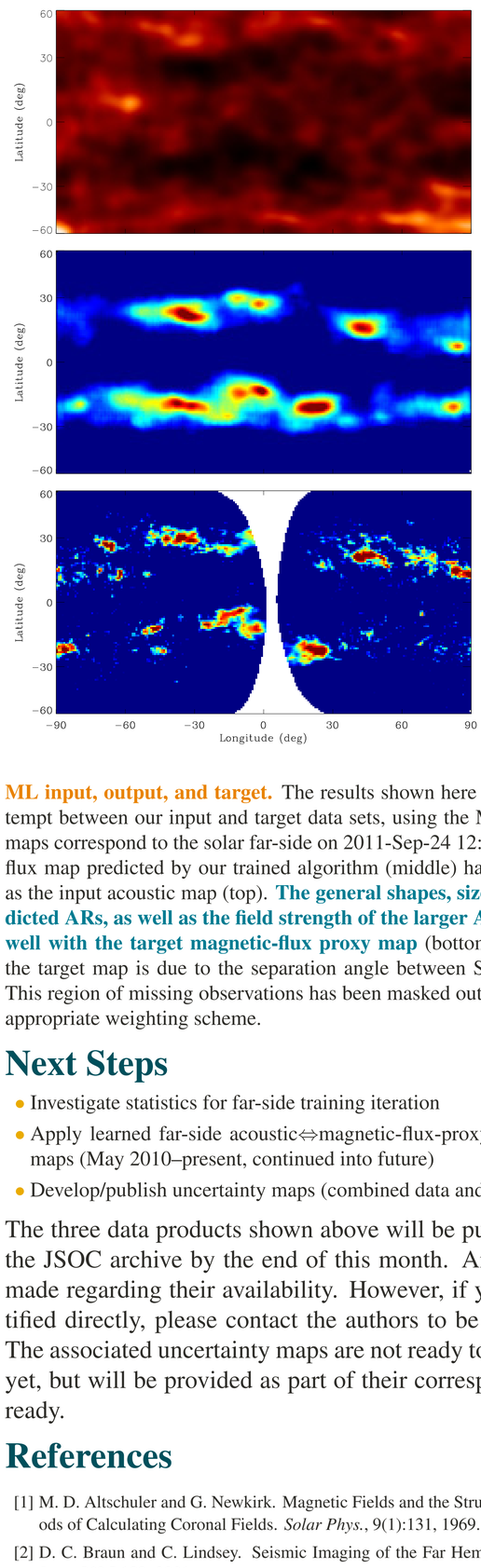

Far Side Acoustic Map

Far Side Acoustically-Derived Magnetic Flux Map

Far Side EUV-Derived Magnetic Flux Map

ML input, output, and target. The results shown here are from the first training attempt between our input and target data sets, using the ML framework above. These maps correspond to the solar far-side on 2011-Sep-24 12:00 UT. The output magnetic-flux map predicted by our trained algorithm (middle) has the same spatial resolution as the input acoustic map (top). **The general shapes, sizes, and locations of the predicted ARs, as well as the field strength of the larger ARs, correspond reasonably well with the target magnetic-flux proxy map** (bottom). The gap in the center of the target map is due to the separation angle between STEREO A & B at the time. This region of missing observations has been masked out of the loss function using an appropriate weighting scheme.

Next Steps

- Investigate statistics for far-side training iteration
- Apply learned far-side acoustic⇔magnetic-flux-proxy relationship to all acoustic maps (May 2010–present, continued into future)
- Develop/publish uncertainty maps (combined data and model sensitivities)

The three data products shown above will be publicly available through the JSOC archive by the end of this month. An announcement will be made regarding their availability. However, if you would like to be notified directly, please contact the authors to be put on a "mailing list". The associated uncertainty maps are not ready to be made available as of yet, but will be provided as part of their corresponding data series once ready.

References

[1] M. D. Altschuler and G. Newkirk. Magnetic Fields and the Structure of the Solar Corona. I: Methods of Calculating Coronal Fields. *Solar Phys.*, 9(1):131, 1969.

[2] D. C. Braun and C. Lindsey. Seismic Imaging of the Far Hemisphere of the Sun. *Astrophys. J. Lett.*, 560:L189, 2001.

[3] J. T. Hoeksema, J. M. Wilcox, and P. H. Scherrer. Structure of the heliospheric curent sheet in the early portion of sunspot cycle 21. *J. Geophys. Res.*, 87(A12):10331, 1982.

[4] C. Lindsey and D. C. Braun. Seismic images of the far side of the sun. *Science*, 287(5459):1799, 2000.

[5] K. H. Schatten, J. M. Wilcox, and N. F. Ness. A model of interplanetary and coronal magnetic fields. *Solar Phys.*, 6(3):442, 1969.

[6] C. J. Schrijver and M. L. DeRosa. Photospheric and heliospheric magnetic fields. *Solar Phys.*, 212 (1):165, 2003.

[7] V. S. Titov. Generalized Squashing Factors for Covariant Description of Magnetic Connectivity in the Solar Corona. *Astrophys. J.*, 660(1):863, 2007.

[8] I. Ugarte-Urra, L. Upton, H. P. Warren, and D. H. Hathaway. Magnetic Flux Transport and the Long-Term Evolution of Solar Active Regions. *Astrophys. J.*, 815(2):90, 2015.

[9] J. Zhao. Time-Distance Imaging of Solar Far-Side Active Regions. *Astrophys. J. Lett.*, 664(2): L139, 2007.

[10] J. Zhao, D. Hing, R. Chen, and S. A. Hess Webber. Imaging the Sun's Far-Side Active Regions Using Multiple Measurement Schemes of Multi-Skip Acoustic Waves. *Astrophys. J. (Accepted)*, 2019.